Red wood-ant nests are traps for fault-related CH_4 micro-seepage

G.M. Berberich[1], A.M. Ellison[2], J. Hartmann[3], M.B. Berberich[4], A. Grumpe[1], A. Becker[1], C. Wöhler[1]

[1]Technical University of Dortmund, Faculty of Electrical Engineering and Information Technology, Image Analysis Group, Otto-Hahn-Straße 4, 44227 Dortmund, Germany; **Corresponding author**: gabriele.berberich@tu-dortmund.de; Tel: +49-231-755-4518 or +49-2235-955233

[2]Harvard University, Harvard Forest, 324 North Main Street, Petersham, Massachusetts, 01366 USA

[3]Institut für Geowissenschaften, Universität Heidelberg, Im Neuenheimer Feld 236, 69120 Heidelberg

[4]IT-Consulting Berberich, Am Plexer 7, 50374 Erftstadt, Germany

Abstract

Methane (CH_4) is common on Earth, forms the major commercial natural gas reservoirs, and is a key component of the global carbon cycle, but its natural sources are not well-characterized. We present a geochemical dataset acquired from a red wood-ant (RWA; *Formica polyctena*) nest in the Neuwied Basin, a part of the East Eifel Volcanic Field (EEVF), focusing on methane (CH_4), stable carbon isotope of methane ($\delta^{13}C$-CH_4), RWA activity patterns, earthquakes, and earth tides. Nest gas and ambient air were analyzed to detect microbial, thermogenic, and abiotic fault-related micro-seepage. Neither methane degassing nor RWA activity was synchronized with earth tides. Two $\delta^{13}C$-CH_4 signatures were identified in nest gas: -69‰ and -37‰. The -69‰ signature of $\delta^{13}C$-CH_4 within the RWA nest is attributed to microbial decomposition of organic matter. This finding supports previous findings that RWA nests are hot-spots of microbial CH_4. Additionally, the -37‰ $\delta^{13}C$-CH_4 signature is the first evidence that RWA nests also serve as traps for fault-related emissions of CH_4. The -37‰ $\delta^{13}C$-CH_4 signature can be attributed either to thermogenic/fault-related or to abiotic/fault-related CH_4 formation originating from e.g. low-temperature gas-water-rock reactions in a continental setting at shallow depths (micro-seepage). Sources of these micro-seeps could be Devonian schists (“Sphaerosiderith Schiefer”) with iron concretions (“Eisengallen”), sandstones, or the iron-bearing “Klerf Schichten”. We cannot exclude overlapping micro-seepage of magmatic CH_4 from the Eifel plume. Given the abundance of RWA nests on the landscape, their role as sources of microbial CH_4 and traps for abiotically-derived CH_4 should be included in estimation of methane emissions that are contributing to climatic change.

Keywords

red wood ants, *Formica polyctena*, CH_4, $\delta^{13}C$-CH_4, fault, activity pattern

Acknowledgements

We thank Daniela Polag (University of Heidelberg) for doing the nest-gas sampling and analyses. RWA activity recording was done using equipment from the Department of Geology at University of Duisburg-Essen. We also thank Dr. Peter Henrich (Leiter der Direktion Landesarchäologie - Außenstelle Koblenz) for his permission to conduct the survey on the Goloring site, and Hans-Toni Dickers, Paul Görgen and Bernd Klug from Kuratorium für Heimatforschung und -pflege, Kobern-Gondorf for their support during the field campaign.

Funding

The study is part of the research project “GeoBio-Interactions” funded by the VW-Stiftung (Az 93 403).

1 Introduction

Methane (CH_4) is common on Earth, forms the major commercial natural gas reservoirs, and is a key component of the global carbon cycle (Keppler et al 2009; Etiope and Sherwood Lollar 2013). This second-most important greenhouse gas currently has an average atmospheric concentration of 1.82 ppm, and continues to increase (Saunois et al. 2016). Today, most natural occurrences of CH_4 are associated with terrestrial and aquatic processes. In the shallow subsurface, CH_4 is produced on geological time scales mainly by thermal conversion of organic matter resulting from heat and pressure deep in the Earth's crust or by microbial activity. This biotic CH_4 includes the formation of thermogenic CH_4 and microbial aceticlastic methanogenesis (Etiope and Schoell 2014; Kiätävienen and Purkamo 2015). In contrast, abiotic CH_4 is produced in much smaller amounts on a global scale and is formed by either high-temperature magmatic processes (Sabatier-type reactions) in volcanic and geothermal areas, or via low-temperature (<100 °C) Fischer-Tropsch-Type (FTT) gas-water-rock reactions in continental settings, even at shallow depths. It is found in specific geologic environments, including volcanic and geothermal systems; fluid inclusions in igneous intrusions; crystalline rocks in Precambrian Shields; and submarine, serpentinite-hosted hydrothermal fields or land-based serpentinization fluids (Etiope and Sherwood Lollar 2013; Etiope and Schoell 2014).

In most geologic environments, biotic and abiotic gases occur simultaneously. Both thermogenic and abiotic CH_4 reach the atmosphere through marine and terrestrial geologic gas (micro-)seeps, and during the exploitation and distribution of fossil fuels. To identify whether locally elevated CH_4 concentrations in the atmosphere are due transportation via fault networks, a determination of possible methane source(s) is required. At the land surface, CH_4 is produced by methanogenic Archaea in anaerobic soil environments or through oxidation by methanotrophic bacteria in aerobic topsoils (Jílková et al. 2016). Isotopic measurements of $\delta^{13}C\text{-}CH_4$ can distinguish abiotic from biotic CH_4 (Schoell 1980; Keppler et al. 2006).

Increase in compressive stress, changes in the volume of the pore fluid or rock matrix, and fluid movement or buoyancy are important mechanisms driving fluid flow and keeping fractures open (Birdsell et al. 2015; Boothroyd et al. 2016). Faults and fracture networks act as preferential pathways of lateral and vertical degassing, creating linear fault-linked anomalies, irregularly-shaped diffuse or "halo" anomalies and irregularly-spaced plumes or "spot anomalies" (e.g. Ciotoli et al. 2006; Etiope 2009). Boothroyd et al. (2016) showed that faults had $\delta^{13}C\text{-}CH_4$ = −37‰ and a significantly higher CH_4 flux

(11.5±6.3 t CH_4 km^{-1} yr^{-1}) than control zones. In Europe, micro-seeps occur both onshore and offshore, with estimated CH_4 flux in Europe of 0.8 Tg yr^{-1} and total seepage of 3 Tg yr^{-1} (Etiope 2009, Kietäväinen and Purkamo 2015).

Recent research has revealed close relationships between the spatial distribution of red wood-ant nests (*Formica rufa*-group; henceforth RWA) and tectonic fault zones (Berberich 2010; Berberich and Schreiber 2013; Berberich et al. 2016; del Toro et al. 2017). Exploratory testing of fault-zone gases revealed that helium (He) and radon (Rn) in RWA nests exceeded atmospheric and background concentrations (Berberich 2010; Berberich and Schreiber 2013; Berberich et al. 2016). However, little consideration has been given to the natural release of CH_4 from RWA nests (Jílková et al. 2016) or via fault zones (Boothroyd et al. 2016), although there are a range of processes that could contribute to it, including micro-seepage via buoyant flux of CH_4, faults increasing the flow rate of microbubbles, and gas vents or response to earth tides and earthquakes (Crockett et al. 2010; Etiope and Klusman 2002).

We used a combination of geochemical, geophysical, and biological techniques; state-of-the-art image analysis; and statistical methods to identify associations between RWA activity, CH_4 degassing, earth tides, and tectonic processes. We explored whether RWA nests are associated with actively degassing faults or traps for migrating CH_4 from the deep underground, and if RWA activity changed during the (micro)-seepage process. Specifically, we tested the null hypotheses that, in the field, RWA activity and concentrations of both CH_4 and $\delta^{13}C$-CH_4 are independent.

2 Methods

We explored associations between RWA activity, methane concentrations in ant nests and ambient air, tectonic events, weather processes, and earth tides at the Goloring site near Koblenz, Germany during an 8-d sampling campaign that ran from 4–11 August 2016.

2.1 Study area

The Goloring site is located west of the Rhine River, southeast of the Laacher See volcano, and close to the Ochtendung Fault Zone in the seismically active Neuwied Basin, which is part of the Quaternary East Eifel Volcanic field (EEVF; western Germany; Fig. 1a). The EEVF includes ≈100 Quaternary volcanic eruption centers; the Laacher See volcano experienced a phreato-plinian eruption ≈12,900 years ago (Litt et al. 2001). The Paleozoic basement consists of alternating strata of Devonian, iron-

bearing, quartzitic sandstones with a carbonate matrix and argillaceous shale reaching to 5-km depths. Several thin black coal seams (Upper Siegen) are embedded within these alternating strata (LGB RLP 2005). Ecocene/Oligocene lignite seams are found at ≈75–160 m and are covered by Paleogene volcanites and Neogene clastic sediments. The study area has been affected by complex major tectonic and magmatic processes, including plume-related thermal expansion of the mantle-lithosphere (Ritter et al. 2001: Walker et al. 2005; Tesauro et al. 2006), crustal thinning and associated volcanism (Clauser 2002), active rifting processes (Hinzen 2003), and possibly crustal-scale folding or the reactivation of Variscan thrust faults under the present-day NW–SE-directed compressional stress field (Hinzen 2003; Dèzes et al. 2004). Those processes can be attributed to the existence of old zones of weakness that are reactivated under the current stress field (Ahorner 1983; Ziegler and Dèzes 2005; Tesauro et al. 2006). Earthquakes (Fig. 1a) are concentrated in areas that are related to the seismically active Ochtendunger Fault Zone (Ahorner 1983). These earthquakes are related to stress-field-controlled block movements, have a weak-to-moderate seismicity, and occur mostly in a shallow crustal depth (≤15 km) with local magnitudes (Richter scale) rarely exceeding 4.0. No fault zones have been reported from our Goloring study site, and focal depth of earthquakes near the site never exceeded 28 km during our sampling campaign (BNS 2016).

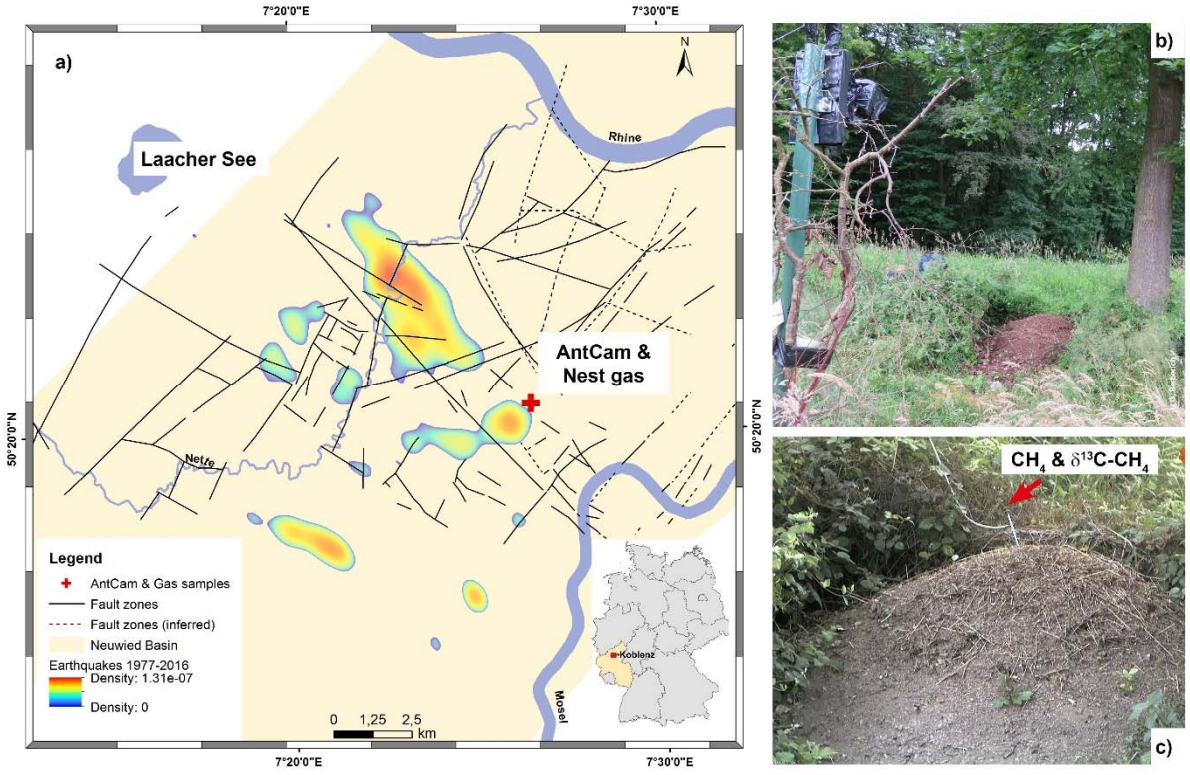

Fig. 1 **Location of the Goloring study area (red cross) ≈15 km SE of the Laacher See volcano within the Neuwied Basin (light yellow area). The map (a) shows tectonic structures (black lines) and probability density of the earthquake events from 1977-2016 which are related to the Ochtendunger Fault Zone (rainbow contours). The inset shows the location of study site within Germany. Photographs show (b) the AntCam for continuous monitoring of ant activity and (c) the nest gas probe (all photographs: G. Berberich)**

2.2 Monitoring red wood ant activity

Within the research project "GeoBio-Interactions" (March – September, 2016), we monitored RWA activity using an "AntCam": a high-resolution camera system (Mobotix MX-M12D-Sec-DNight-D135N135; 1,280 × 960 pixels) installed ≈5 m from a RWA nest (Fig. 1b). During the 192-hr CH_4 sampling campaign, which ran from 4–11 August, 2016, ant activities were recorded and time-stamped continuously (12 Hz). The network-compatible AntCam was connected to a network-attached storage (NAS) system for data storage via a power-over-Ethernet (POE) supply. A computer connected to the NAS evaluated the RWA activities on-site and in real time using C++ code to accelerate image evaluation. Image analysis extended the system of Berberich et al. (2013) and was based on the difference image technique (Fig. 2). To reduce negative influences caused by, e.g., moving blades of grass, we used a mask to restrict analysis to only the visible top of the mound. To compensate for slight movements of the camera, e.g., due to wind, an image registration of the current image relative to the previous image was done based on mutual information before the determination of the absolute difference image (Maes et al. 1997). Results of RWA activity were written to a file. Every hour, this file was sent via email (mobile data transfer, LTE router) to a mail server. Since two different sensors were used for the day and night, respectively, we computed different polynomials to map the sum of absolute differences onto manually designed activity categories in a follow-up procedure. The coefficients of the polynomials were obtained from a minimization of the sum of squared differences between the polynomial model and the manually assigned category for two selected weeks. A first-order polynomial was adapted to the daytime data and a third-order polynomial was adapted to the nighttime data. To avoid numerical difficulties, we first centered and scaled the data by subtracting the mean of the data during the target time and dividing by the standard deviation. Both values were computed for day- and nighttime, respectively.

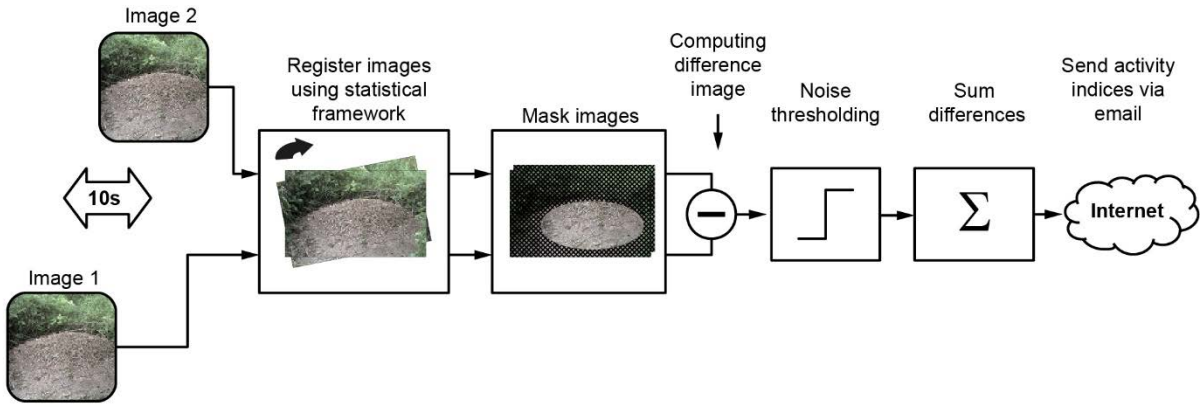

144

145 **Fig. 2 Workflow for acquisition and estimation of RWA activity**

146 2.3 Gas sampling and geochemical analyses

147 Field measurements of CH_4 were taken from 4–11 August 2016. A stainless-steel probe (inner diameter
148 0,6 cm) was inserted into the *F. polyctena* nest to a depth of 80 cm and remained there, unmoved,
149 during the entire 192-hour sampling campaign. The probe was used for continuous CH_4/$\delta^{13}C$-CH_4
150 measurements. The probe was equipped with a flexible tip attached to a pushable rod and a sealable
151 outlet for docking sampling equipment. The closed probe was inserted into the nest. After opening by
152 pushing the rod, the probe was evacuated twice, using a 20-ml syringe. After this, the outlet was closed
153 to prevent atmospheric influence. The outlet was only opened after docking the sampling unit to it.

154 Concentrations of CH_4 and $\delta^{13}C$-CH_4 in nest gas (NG) and ambient air (AA) were monitored using a
155 portable CRDS analyser (G2201-i; Picarro, USA) that measured $^{12}CH_4$, $^{13}CH_4$ and H_2O quasi-
156 simultaneously at 1 Hz, and provided $\delta^{13}C$ values relative to the Vienna Pee Dee Belemnite standard.
157 The G2201-i uses built-in pressure and temperature control systems, and automatic water-vapor
158 correction to ensure high stability of the portable analyzer. Effects of water vapor on the measurement
159 were corrected automatically by the Picarro® software. The manufacturer guarantees concentration
160 precision for the analysis of CH_4 in the “high precision mode” of 5 ppbv ± 0.05 % (^{12}C) and 1 ppbv ±
161 0.05% (^{13}C) within a concentration range of 1.8–1000 ppm. The guaranteed precision of $\delta^{13}C$-CH_4 is
162 <0.8‰.

163 The CRDS analyzer was deployed in a dry, wind-sheltered location near the RWA nest. Nest gases
164 were pumped from the aforementioned probe into the CRDS analyzer for analysis of CH_4 and $\delta^{13}C$-CH_4

values. Ambient air was measured 2 m away from the nest for 15 min every four hours during the operation using a 3-way-valve, avoiding disturbance of the nest or the position of the steel probe. All gases passed through a chemical trap filled Ascarite® (sodium hydroxide coated silica; www.merckgroup.com) before entering the system to remove carbon dioxide (CO_2) because the high concentrations of CO_2 in the nest samples could interfere with the measurements of CH_4 and $\delta^{13}C\text{-}CH_4$. Gas samples were dried by a Nafion® drying tube (Nafion MD110, PermaPure LLC, USA) before measurements to ensure higher accuracy and subsequently analyzed for CH_4 concentration and $\delta^{13}C\text{-}CH_4$. To assure quality of the CH_4 and $\delta^{13}C\text{-}CH_4$ values, reference gas measurements were taken every 8 h during the operation. Fluctuations in atmospheric CH_4 and $\delta^{13}C\text{-}CH_4$ values were validated against a single, 4-h measurement of ambient air. Carbon isotope ratios are expressed using standard delta (δ) notation as described by deviations from a standard: $\delta_{sample}‰ = ((R_{sample}/R_{standard} -1)) \times 1000$, where R is the $^{13}C/^{12}C$ ratio in the sample or standard. A total of 459 704 samples for both CH_4 and $\delta^{13}C\text{-}CH_4$ in nest gas and 27 samples in ambient air were collected and analyzed.

2.4 Meteorological Parameters

A radio meteorological station (WH1080) placed 2 m above the ground at the Goloring site continuously logged meteorological conditions (temperature [°C], humidity [%], air pressure [hPa], wind speed [m/s], rainfall [mm], and dew point [°C]) at 5-min intervals. The recorded data were downloaded every two days, checked for completeness, and stored in a data base.

2.5 Earthquake events

Data on earthquake events during the sampling campaign were obtained from the seismological databases provided by the Erdbebenstation Bensberg (BNS, www.seismo.uni-koeln.de/events/index.htm) and by the Landesamt für Geologie und Bergbau, Rheinland-Pfalz (LGB RLP, http://www.lgb-rlp.de/fachthemen-des-amtes/landeserdbebendienst-rheinland-pfalz/). The probability density of the earthquake events was estimated using the kernel density estimator of Kristan et al. (2011) using Gaussian kernels.

2.6 Earth tides

Cyclic changes in the earth's environment are caused by the gravitational pull of both the Sun and the Moon on the earth. These result in two slight lunar and two solar tidal bulges (“earth tides”). The two bulges occur at the surface of the earth that approximately faces the Moon and at the opposite side

while the Earth rotates around its axis. Earth tides were calculated using the tool developed by Dehant et al. and D. Milbert version 15.02.2016 (http://geodesyworld.github.io/SOFTS/solid.htm).

2.7 Data analysis

All analyses were done using R version 3.3.2 (R Core Team 2016) or MATLAB R2017a.

We examined associations between the six measured meteorological variables and RWA activity and CH_4 concentrations. As many of these variables were correlated with one another, we used principal components analysis (R function prcomp) on centred and scaled data to create composite "weather" variables (i.e., principal axes) that were used in subsequent analyses.

We used the "median+2MAD" method (Reimann et al. 2005) to separate true peaks in CH_4 concentrations from background or naturally-elevated concentrations: any observation greater than the overall median+2MAD (2.31 ppm CH_4 in nest gas and 2.11 ppm CH_4 in ambient air) was considered to be a peak concentration. Background and elevated CH_4 concentrations were separated based on the 90% quantile of the CH_4 concentration (Phillips et al. 2013). For $\delta^{13}C$-CH_4, we considered concentrations $< -35‰$ or $> 0‰$ to be peak concentrations. Only peaks occurring in both data sets at the same time were considered to be true peaks. The Keeling plot method (Pataki et al. 2003) was applied to determine the carbon-isotope composition of the found peaks to obtain insights into the processes that govern the distinction between isotopes in the ecosystem.

3 Results

3.1 Meteorological conditions

During the one-week field campaign in August 2016, air temperatures ranged from 5.7–29.1 °C (mean = 16.2 °C), with only 2.1 mm rainfall overnight between 9 and 10 August. Variation in atmospheric pressure (mean 988 ± 2.24 hPa) and wind speed (1.67 ± 1.72 km/h) were small. The first three axes derived by the principal components analysis accounted for nearly 80% of the variance in the data (Table 1). The first axis represents temperature and humidity, the second axis represents atmospheric pressure (with additional contributions of humidity and windspeed), and the third axis represents rainfall and windspeed (with a minor contribution of temperature).

Table 1 **Results of the principal components analysis of the measured weather variables. Values in the first six rows are the loadings of each variable on each of the first three principal axis; only loadings > |0.3| are shown. The last row of the table gives the cumulative proportion of the variance explained by each of the first three principal axes**

Variable	PC-1	PC-2	PC-3
Temperature (°C)	−0.69		0.3
Atmospheric Pressure (hPa)		0.62	
Dew-point (°C)	−0.43	0.49	
Relative humidity (%)	0.48	0.45	
Rainfall (mm)			0.77
Windspeed (km/h)		−0.41	0.50
Cumulative variance explained	0.34	0.59	0.77

220

221 ## 3.2 RWA activity

222 Ants were most active during the late afternoon and early evening hours (Fig. 3). The video streams
223 showed that the ants went on foraging, building and maintaining the nest as they had done since the
224 start (on March, 18th) of our longer 7-month field campaign. Decomposition of the time-series into its
225 additive components illustrated that during the one-week gas-sampling campaign, there was a trend
226 towards increasing activity over the first four days, followed by a sharp decline towards the end of the
227 week (Fig. 3). There were two noticeable peaks of activity, at mid-day and early afternoon, followed by
228 sharp spikes in activity near 16:30 hours (Fig. 3).

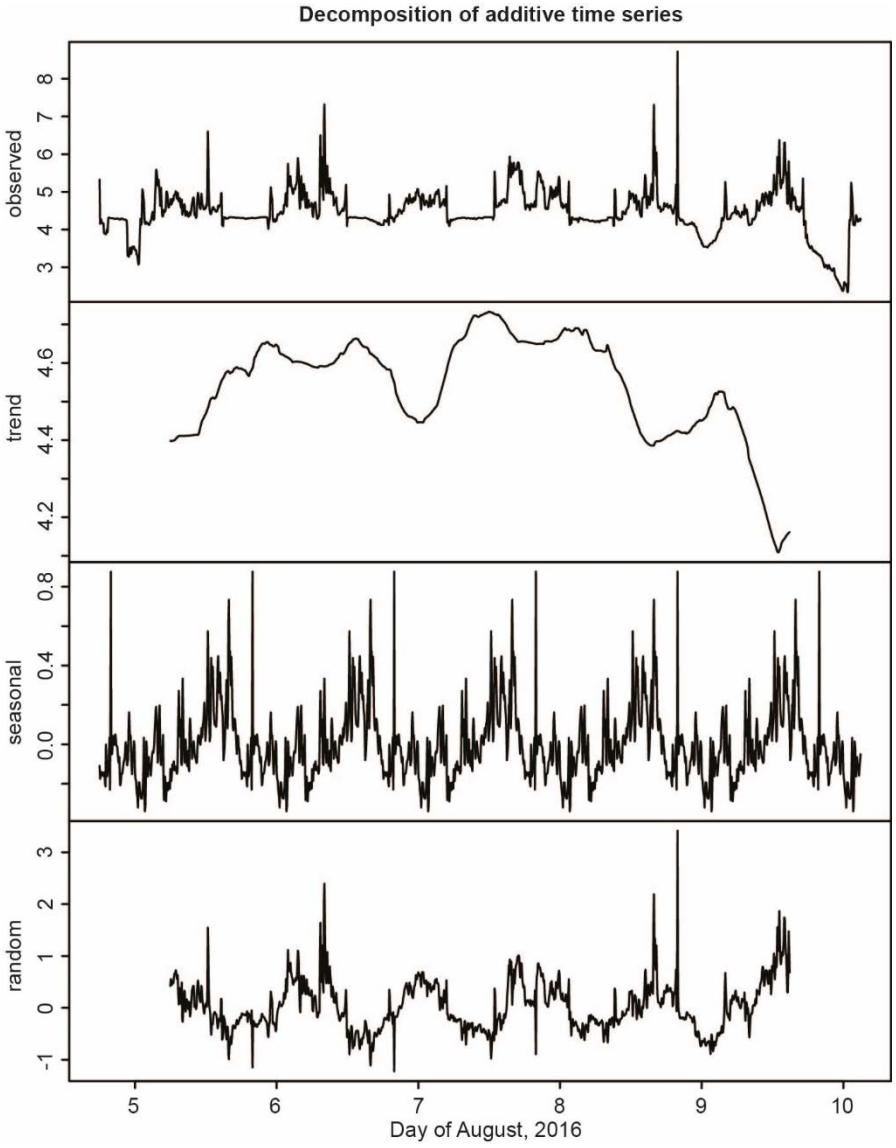

Fig. 3 **Additive time-series decomposition of median RWA activity. An extreme spike in ant activity (observed = 12 units on 04-August at 19:14 UTC and 25 units on 04-August at 19:19 UTC) are not shown to enhance clarity of the "observed" time-series**

No nuptial flight happened during this week. Ventilation phases of the nest took place in the early morning (6:40 – 7:30 UTC) on 5 August for 50 minutes and on 7 August for 20 minutes (6:40 – 7:00 UTC) after sunrise with varying ant activities (Fig. 4). On two days (07.08. and 09.08.), at 04:30 and 05:50 (UTC), respectively, golden hammer birds (*Emberiza citronella*) were "anting" for ≈5 min to kill parasites on their feathers with formic acid; a mouse was observed on the nest at 22:00 (UTC) for 10 minutes on 04.08.16. Only one earthquake occurred nearby (local magnitude: 0.8; depth: 3 km; distance: 20 km). This micro-earthquake neither influenced degassing nor RWA activity.

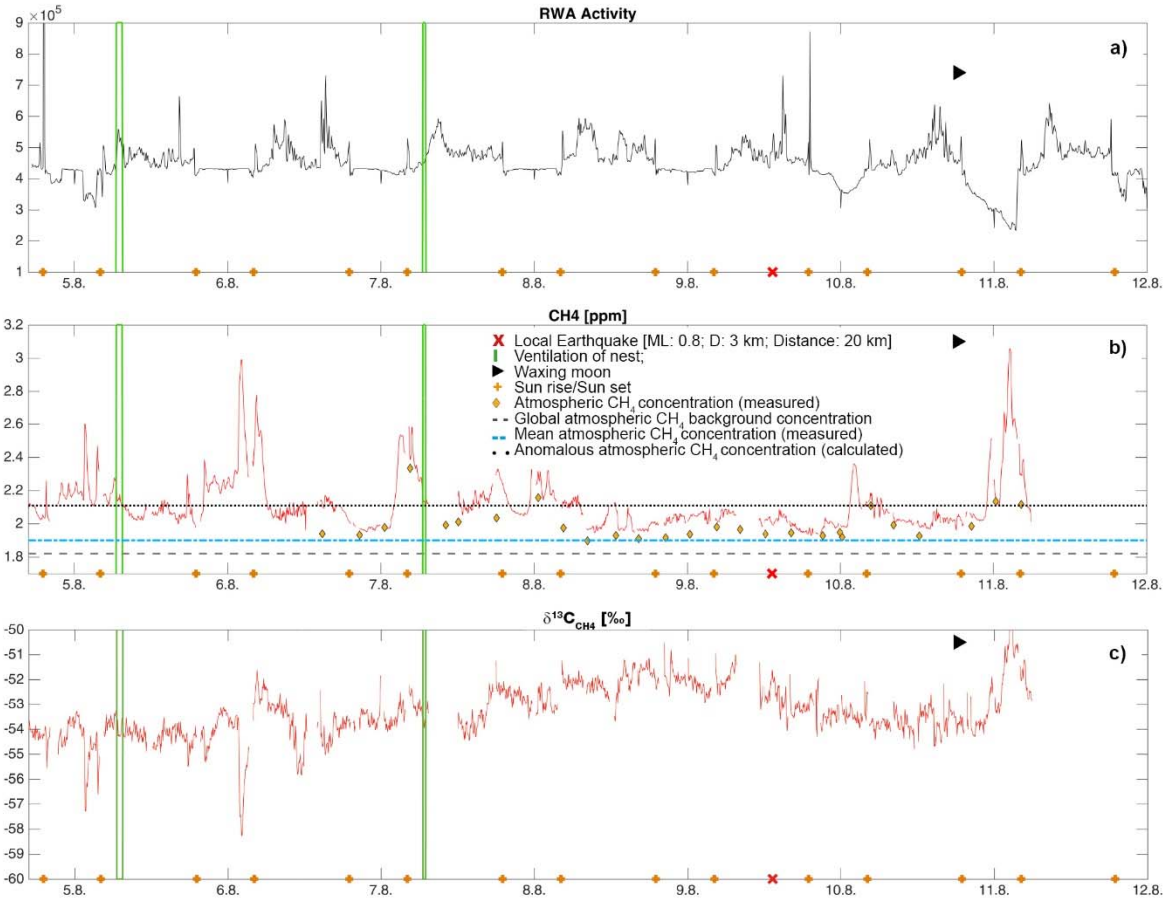

Fig. 4 **Time-series plots of median RWA activities (a), CH_4 (b), and $\delta^{13}C$-CH_4 (c) in nest gas, ventilation phases (green lines) of the nest, sunrise/sunset (orange crosses), and a single local earthquake (red cross) during the sampling week in August 2016. Reference lines indicate the global atmospheric CH_4 background concentration (Saunois et al. 2016; black dashed line), the local mean CH_4 atmospheric concentration (blue dotted line), and the calculated anomalous atmospheric CH_4 concentration (black dotted line)**

Median RWA activity and the three principal axes of weather were modestly associated, and accounted for only 8% of the variance in ant activity (Table 2). The ant activity increased slightly at lower temperatures (PC-1) and slightly decreased when rainfall (PC-3) was present. PC-2 was not associated significantly with RWA activity.

Table 2 **Summary ANOVA table of the linear model examining the effects of weather conditions on median RWA activity. The estimate is the slope describing the relationship between each principal component and median RWA activity. The remaining columns are the degrees of**

freedom, mean square, and F-statistic for each term in the model. (*$P < 0.001$; $^{NS}P > 0.5$). Overall model $r^2 = 0.08$; $F_{3,1536} = 47.57$, $P < 0.001$**

	Estimate	Df	MS	F
PC-1	0.19	1	110.8	120.6***
PC-2	−0.01	1	0.3	0.3^{NS}
PC-3	−0.11	1	20.0	21.8***
Residual		1563	0.9	

3.3 CH_4 and $\delta^{13}C$-CH_4 in nest gas

Concentrations of CH_4 in the nest exceeded the global atmospheric background concentration (1.82 ppm; Saunois et al. 2016) and ranged from 1.93 to 3.07 ppm (Fig. 4 and Table 5). $\delta^{13}C$-CH_4 ranged from −58.48 to −49.54‰ (Fig. 5). Atmospheric CH_4 concentrations were slightly variable (1.90 – 2.33 ppm). The calculated anomalous threshold concentration for atmospheric CH_4 was 2.11 ppm CH_4 (Fig.4). Only four measurements out of 27 exceeded this threshold. Weather conditions explained 22% of the variation in $\delta^{13}C$-CH_4 (‰), and decreased with all measured weather variables (Table 4).

Table 3 Summary ANOVA table of the linear model examining the effects of weather conditions on CH_4 concentration (ppm). The estimate is the slope describing the relationship between each principal component and CH_4 concentration. The remaining columns are the degrees of freedom, mean square, and F-statistic for each term in the model. (*$P < 0.001$; *$P < 0.5$). Overall model $r^2 = 0.19$; $F_{3,1536} = 121.5$, $P < 0.001$**

	Estimate	Df	MS	F
PC-1	−0.3	1	263.1	323.8***
PC-2	0.1	1	29.8	36.6***
PC-3	0.04	1	3.4	4.1*
Residual		1563	0.8	

Table 4 Summary ANOVA table of the linear model examining the effects of weather conditions on $\delta^{13}C$-CH_4 (‰). The estimate is the slope describing the relationship between each principal

component and CH_4 concentration. The remaining columns are the degrees of freedom, mean square, and F-statistic for each term in the model. (*$P < 0.001$). Overall model r^2 = 0.22; $F_{3,1536} = 149.5$, $P < 0.001$**

	Estimate	Df	MS	F
PC-1	0.22	1	153.2	196.8***
PC-2	−0.24	1	137.8	177.0***
PC-3	−0.19	1	58.2	74.8***
Residual		1563	0.8	

Eight significant peaks in nest gas were found for CH_4 and $\delta^{13}C\text{-}CH_4$ (Fig. 5a, b). These peaks occurred between 17:39 (UTC) and 06:54 (UTC) the following day, but were otherwise not temporally predictable. Results of the Keeling plots (Pataki et al. 2003) revealed two signatures for $\delta^{13}C\text{-}CH_4$ at −37‰ and −69‰ in nest gas (Fig. 5c).

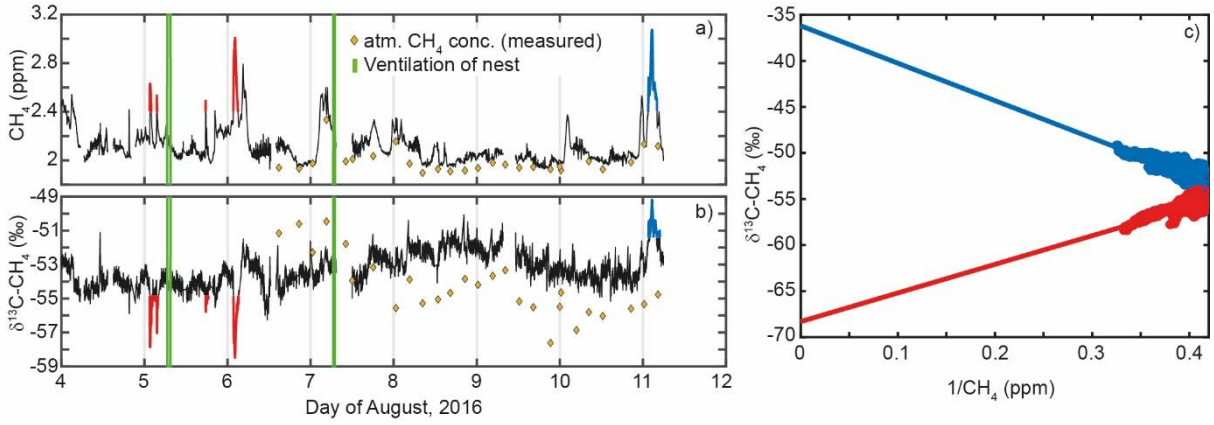

Fig. 5 Peak concentrations in CH_4 (a) and $\delta^{13}C\text{-}CH_4$ (b) and Keeling plot of $\delta^{13}C\text{-}CH_4$ (c) from nest gas. Note the peaks indicate two signatures for $\delta^{13}C\text{-}CH_4$ in nest gas at −37‰ and −69‰ (c)

Joint visualization of the time series of ant activity, methane concentrations, and weather reveal that all the time series exhibited a periodicity of approximately 24 hours. (Fig. 6), and cross-correlations showed positive and negative peaks at daily intervals. The absolute value of the cross-correlation coefficient ≤ 0.3, and the strongest cross-correlation occurred at a lag of ≈−30 minutes, less than the original filter width of the ant activity time series.

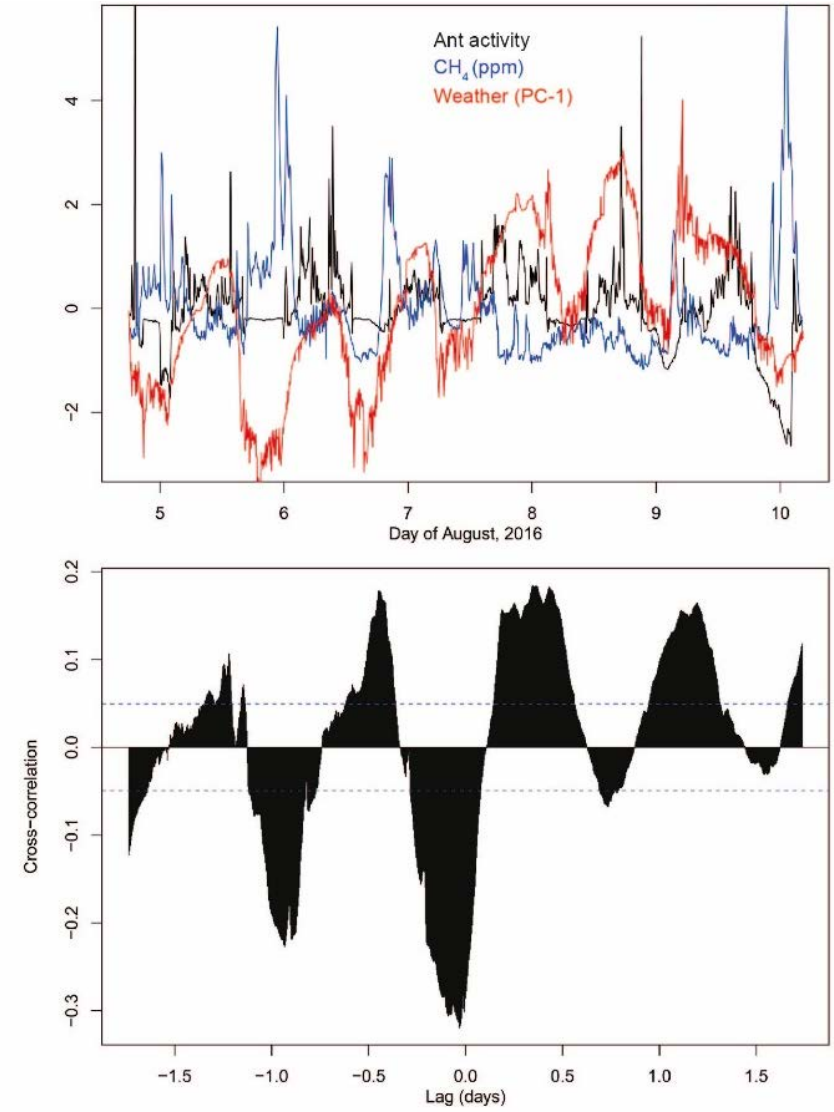

Fig. 6 **Top: Time-series plot of median ant activity (black), methane concentration (blue), and weather conditions (PC-1, red). All values are centered and scaled (i.e., are reported in SD units). Bottom: Cross-correlation between median ant activity and methane activity**

3.4 Earth tides

Earth tides were basically semi-diurnal, and we observed a slight increasing trend in amplitude during the intensive sampling period (Fig. 7, top). The cross-correlation between ant activity and earth tides never exceeded 0.25 (Fig. 7, bottom). Methane activity (Fig. 8) showed a correlation-coefficient with earth tides of ≈−0.4 at a lag of 6–8 hours. The cross-correlation between the earth tides and $\delta^{13}C\text{-}CH_4$ was ≤ |0.15| (Fig. 8, bottom).

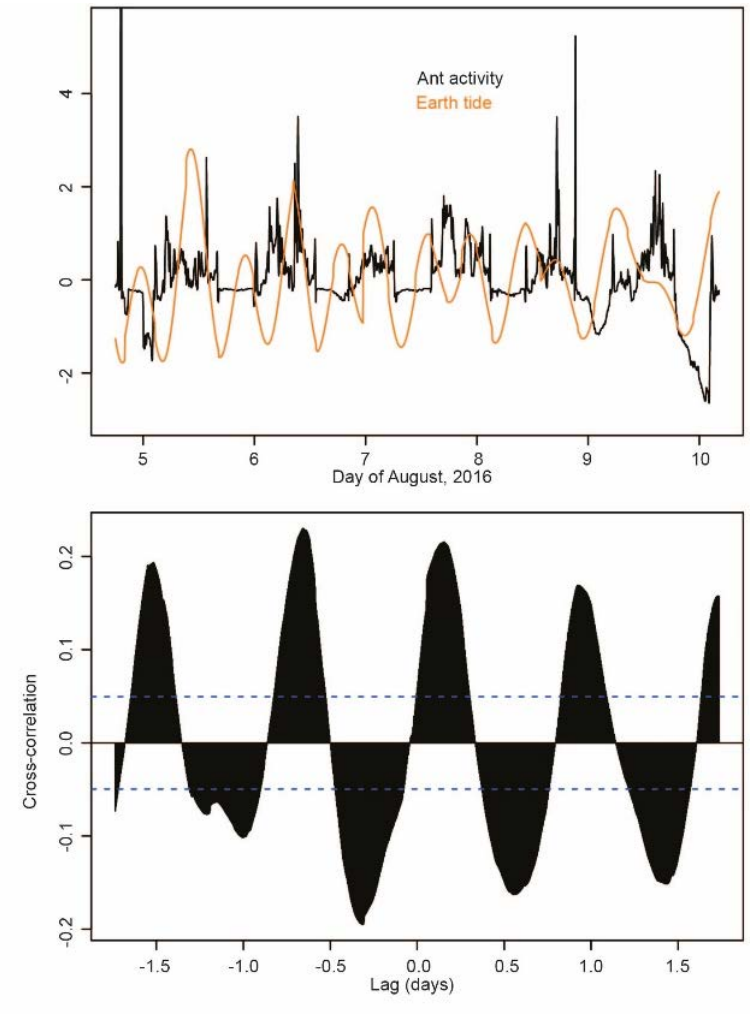

283

284 **Fig. 7** **Relationships between ant activity and earth tides. Top: time-series of centered and scaled**

285 **data. Bottom: cross-correlation of the time-series of ant activity and earth tides**

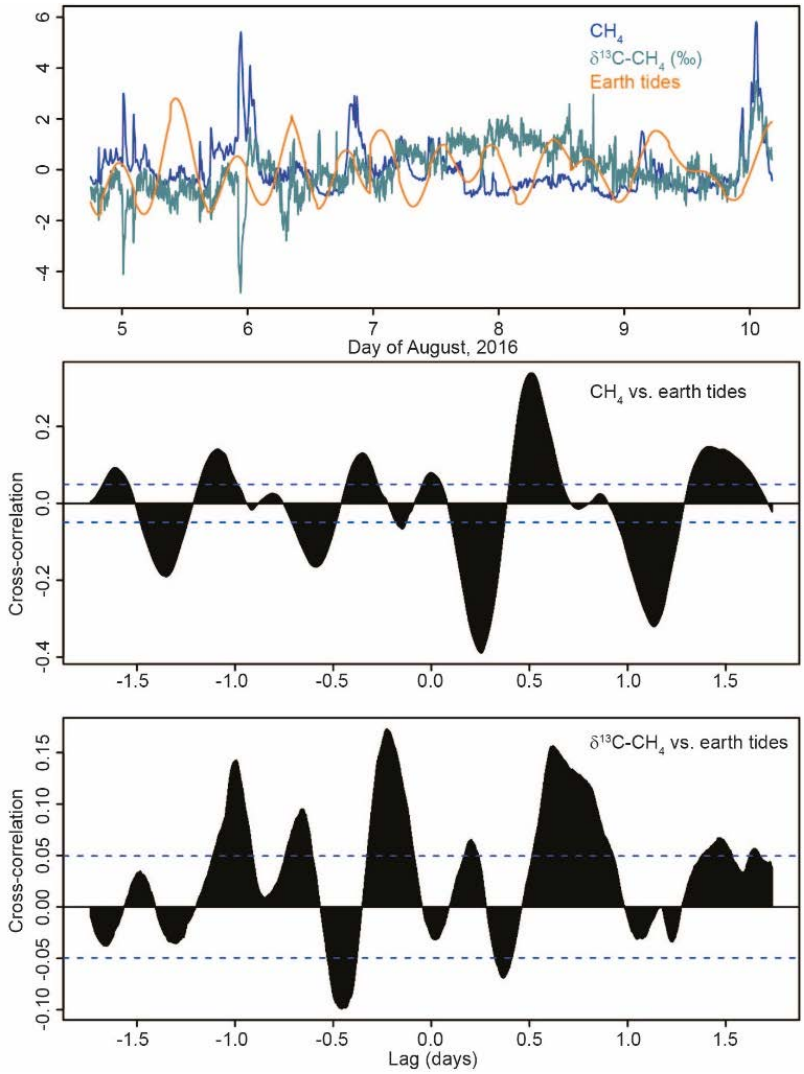

Fig. 8 **Relationships between CH_4 (blue), $\delta^{13}C\text{-}CH_4$ (green), and earth tides (orange). Top: time-series of centered and scaled data. Middle and bottom: cross-correlation of the time-series of CH_4 and $\delta^{13}C\text{-}CH_4$ with earth tides**

4 Discussion

4.1 Meteorological Conditions

Meteorological conditions were stable during the sampling week. Variation in atmospheric pressure was small and there was almost no rainfall. Less than 25% of the variance in CH_4 and $\delta^{13}C\text{-}CH_4$ were accounted for by weather conditions (*cf.* Toutain and Baubron 1999).

4.2 RWA activities

During the investigation period, ant activity was higher than we had observed in 2009-2012, although an “M-shaped” pattern in daily activity was still identifiable (Berberich et al. 2013). Relatively high RWA activities during the late afternoon and early evening hours could be attributable to direct sun hitting the nest during that time or with activities associated with rebuilding damage to the nest that had occurred on 18 March. Additional external agents, including mice and “anting” birds, did not influence ant activities during the sampling week. Ant activity was only weakly correlated with weather (see also Berberich et al. 2013) or methane seepage.

4.2 CH_4 and $\delta^{13}C$-CH_4 in nest gas

Measured atmospheric CH_4 concentrations were always lower than CH_4 in RWA nests and there seemed to be little influence of atmospheric CH_4 on CH_4 in the nests. Rather, elevated CH_4 concentrations in nest gas appear to result from a combination of microbial activity and transport through fault networks. Comparison of $\delta^{13}C$-CH_4 nest gas signatures with published data suggests that it can be attributed to two different sources (Fig. 9).

The $\delta^{13}C$-CH_4 signature of −69‰ in nest gas indicates a microbial source, such as decomposing organic matter that is high in nutrients (Keppler et al. 2006; Jílková et al. 2016). This result supports the findings of Jílková et al. (2016) that the aboveground parts of wood ant nests are hot-spots of CH_4 production.

The second isotope signature, −37‰ $\delta^{13}C$-CH_4, can be attributed either to thermogenic/fault-related (Boothroyd et al. 2016) or to abiotic/fault-related CH_4 formation (Etiope et al. 2016). Boothroyd et al. (2016) found a $\delta^{13}C$-CH_4 signature of −37‰ for fugitive emission of CH_4 via migration along fault zones in the United Kingdom. Our result of -37‰ $\delta^{13}C$-CH_4 is of the same order (Table 5) and can be attributed to fault-related CH_4 emission moving through the RWA nest.

Continental loss of volatiles requires tectonically active parts and the formation of fluid-filled conduits through the continental crust. Suitable locations can be found in extensional regimes and their related volcanism (Clauser 2002), such as are present in our study area. Gas permeable faults and fractured rocks are pathways to naturally release significant amounts of "old" CH_4 of crustal origin. Significant geologic CH_4 emissions, comprising both biogenic and thermogenic CH4, are due to hydrocarbon production in sedimentary basins and, subordinately, to inorganic Fischer-Tropsch type reactions occurring in geothermal systems (Etiope and Klusmann 2002). A variety of geological, chemical and

biological processes have impacts on the deep carbon cycle. There are three possible sources for the fault-related CH_4 we find in RWA nests.

Table 5 Descriptive statistics for nest gas CH_4 (ppm) at Goloring site compared to fugitive emissions of CH_4 (ppm) from basin bounding faults in the UK (Boothroyd et al. 2016). SE = 1 standard error of the mean

Data amount	Location	Target	N	Mean	SE	Min	Max
All data	Widmerpool	Fault	8313	1.91	0.000395	1.89	2.80
	Lancashire	Fault	5568	1.88	0.00041	1.87	3.18
	Butterknowle	Fault	9283	1.87	0.000342	1.86	3.97
	90 Fathom	Fault landfill	9374	2.24	0.0151	1.86	13.73
	90 Fathom	Fault no landfill	8537	1.89	0.000452	1.86	2.52
	Vale of Eden	Fault	8428	2.20	0.00169	1.87	4.88
This Study	**Goloring site**	**Nest gas**	**459704**	**2.13**	**0.000238**	**1.93**	**3.07**
Data >90th percentile	Widmerpool	Fault	5	2.34	0.0579	2.24	2.56
	Lancashire	Fault	6	2.56	0.139	2.32	3.18
	Butterknowle	Fault	3	2.34	0.0233	2.29	2.36
	90 Fathom	Fault landfill	692	5.74	0.119	13.73	13.73
	90 Fathom	Fault no landfill	11	2.25	0.0101	2.31	2.31
	Vale of Eden	Fault	2234	2.32	0.00188	2.22	3.23
This Study	**Goloring site**	**Nest gas**	**47147**	**2.50**	**0.00079**	**2.32**	**3.07**

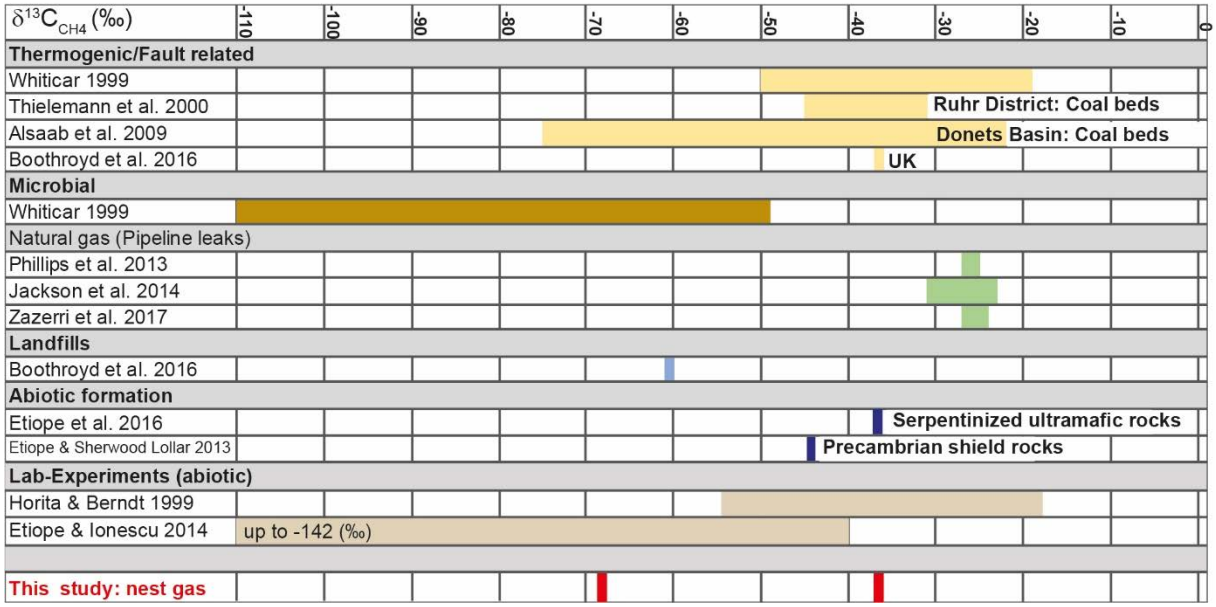

Fig. 9 Comparison of $\delta^{13}C$-CH_4 in nest gas signatures to published data

First, carboniferous coals are sources of thermogenic coalbed methane (CBM) in numerous basins, including the Ruhr and Donets Basins. Their $\delta^{13}C$ are values between -20‰ and -75‰ (Witicar 1999,

334 Thielemann et al. 2000, Alsaab 2009; Fig. 9). Both basins have coal thicknesses of ≈100 m
335 (EnergieAgentur NRW 2009; Alsaab 2009). In our study area, much older Devonian coal seams with
336 very small thicknesses (LGB RLP 2005) are reported at depths up to 9000 m. Though the study area is
337 situated in a suitable tectonic compression/extensional regime, any thermogenic CH_4 would likely be
338 small because of the very low thickness of the seams and might not even lead to measurable coal-bed
339 CH_4 concentrations in nest gas. On the other hand, lignite and coal formations are often associated with
340 aerobic methylotrophs at depths of over 1 km and are usually considered to be anaerobic (Mills et al.
341 2010; Stępniewska and Kuźniar 2013; Stępniewska et al. 2014). In the study area, several small lignite
342 seams (Middle to Upper Eocene) with a thickness of up to 5 m are found in depths of approx. 75 to 160
343 m. The low thickness and the shallow depth of the lignite may not lead to thermogenic CH_4 seepage.

344 Second, $\delta^{13}C\text{-}CH_4$ in land-based serpentinized ultramafic rocks can be as light as −37‰, and methane
345 from Precambrian shields may exhibit even lower values (-45‰; Etiope and Sherwood Lollar 2013;
346 Etiope and Schoell 2014; Etiope et al. 2016). Laboratory experiments have produced abiotic methane
347 with a wide range of $\delta^{13}C\text{-}CH_4$ signatures, including isotopically “light” values once thought to be
348 indicative of biological activity (e.g. −19 to −53.6‰ by Horita and Berndt 1999; −41 to −142‰ by Etiope
349 and Ionescu 2015). Abiotic CH_4 can be mistaken for biotic CH_4 of microbial or thermogenic origin
350 because minor amounts of abiotic gas in biotic gas may prevent its recognition based on C and H isotope
351 analysis (Etiope et al. 2015; Etiope et al. 2016). Sources of abiotic CH_4 formation in the study area can
352 be attributed to magmatic CH_4 formation due to late magmatic (<600°C) re-distribution of C-O-H fluids
353 during magma cooling or gas-water-rock-interactions even at low temperatures and pressures (Etiope
354 and Sherwood Lollar 2013). In the study area, the magmatic source for magmatic CH_4 formation could
355 be the so called “Eifel plume”, a region of about 100-120 km in diameter between 50-60 km depth and
356 at least 410 km depth beneath the study area. The buoyant Eifel plume is characterized by excess
357 temperature of 100–150 K, has approx. 1% of partial melt and is the main source of regional Quaternary
358 volcanism (Ritter 2007).

359 Third, gas-water-rock-interactions, including dissolution of C- and Fe-bearing minerals in water at ~300
360 °C and carbonate methanation between 250 and 800 °C, do not depend on magma or magma-derived
361 fluids (Etiope and Scherwood-Lollar 2013; Kietäväinen and Purkamo 2015). The “Klerf Schichten”
362 (Lower Ems) are alternating layers of reddish Fe-bearing sandstones and C-bearing shales and schists
363 ≤ 2200-m thick and may be suitable formations for decomposition of C- and Fe-bearing minerals.

364 Paleozoic bedrock sediments, especially the “Sphaerosiderith Schiefer” (Upper Ems; ≤ 150-m thick)
365 schists with iron concretions (“Eisengallen”), are suitable formations for carbonate methanation: the
366 decomposition of carbonate minerals (calcite, magnesite, siderite) at lower temperatures in H_2-rich
367 environments without mediation of gaseous CO_2 (as it is usually the case for catalytic hydrogenation or
368 FTT reaction; Etiope and Scherwood-Lollar 2013). Within the habitable zone in the upper crust, at
369 temperatures >150 °C and in the presence of CO_2, CO, and H_2, CH_4 may be produced in aqueous
370 solution even in the absence of a heterogeneous catalyst or gas phase by a series of redox reactions
371 leading to the formation of formic acid, formaldehyde and methanol. Finally, abiotic CH_4 also can form
372 *in situ* through low temperature processes including the Sabatier and Fischer-Tropsch type (FTT)
373 synthesis reactions with metals like Fe or Ni or clay minerals as catalysts (Etiope and Scherwood-Lollar
374 2013: Kietäväinen and Purkamo 2015).

375 Because the largest quantities of abiotic gases found on Earth’s surface are produced by low-
376 temperature gas–water–rock reactions (Etiope et al. 2015) we attribute the −37‰ δ^{13}C-CH_4 signature
377 in RWA nests to fault-related emissions of abiotically formed CH_4 by gas-water-rock reactions occurring
378 at low-temperatures in a continental setting at shallow depths (micro-seepage). Probable sources might
379 be Devonian schists (“Sphaerosiderith Schiefer”) with iron concretions (“Eisengallen”) sandstones
380 and/or the iron-bearing “Klerf Schichten”. However, we cannot exclude the possibility of overlap by
381 magmatic CH_4 micro-seepage from the Eifel plume.

382 The −37‰ δ^{13}C-CH_4 signature in nest gas was detected only once. The micro-earthquake on August 9
383 did not influence CH_4 degassing because of its far distance (20 km). On August 13, there was another
384 earthquake (ML: 0.7; D = 13 km) only 2.3 km away from the nest. It might be, that the −37‰ δ^{13}C-CH_4
385 signature in nest gas was a precursor to the August 13 earthquake, promoting degassing due to an
386 increase in compressive stress (Boothroyd et al. 2016; Birdsell et al. 2015). But this remains unanswered
387 as the CH_4 measurement campaign was terminated at August 11.

388 We suggest that future work seek to determine if the −37‰ signature can be attributed to a microbial
389 source, a purely abiotic source, or a combination of abiotic/thermogenic source. Such a study should
390 use additional measurements of δ^{13}H and run long enough to determine the influence of irregularly timed
391 earthquake events on patterns of methane degassing.

392

5 References

Ahorner L (1983) Historical seismicity and present-day microearthquake activity in the Rhenish Massif, Central Europe. In: Fuchs K, von Gehlen K, Mälzer H, Murawski H and Semmel A. (eds) Plateau Uplift. The Rhenish Shield - A Case History. Springer-Verlag, Berlin, pp 198-221

Alsaab D, Elie M, Izart A, Sachsenhofer RF, Privalov VA, Suarez-Ruiz I, Martinez L, Panova EA (2009) Distribution of thermogenic methane in Carboniferous coal seams of the Donets Basin (Ukraine): "Applications to exploitation of methane and forecast of mining hazards". Int J Coal Geol 78: 27–37

Berberich G (2010) Identifikation junger gasführender Störungszonen in der West- und Hocheifel mit Hilfe von Bioindikatoren. Dissertation. University of Duisburg-Essen

Berberich G, Berberich M, Grumpe A, Wöhler C, Schreiber U (2013) First Results of 2.5 Year Monitoring of Red Wood Ants' Behavioural Changes and Their Possible Correlation with Earthquake Events. Animals. doi:10.3390/ani3010063

Berberich G, Grumpe A, Berberich M, Klimetzek D, Wöhler C (2016) Are red wood ants (*Formica rufa*-group) tectonic indicators? A statistical approach. Ecol Ind. doi:10.1016/j.ecolind.2015.10.055

Berberich G, Schreiber U (2013) GeoBioScience: Red Wood Ants as Bioindicators for Active Tectonic Fault Systems in the West Eifel (Germany). Animals. doi:10.3390/ani3020475

Birdsell DT, Rajaram H, Dempsey D, Viswanathan HS (2015) Hydraulic fracturing fluid migration in the subsurface: a review and expanded modeling results. Water Resour. Res. 51: 7159–7188.

BNS (2016) Earthquake Data Catalogue. Department of Earthquake Geology of Cologne University. www.seismo.uni-koeln.de/catalog/index.htm. Accessed 01 September 2016

Boothroyd IM, Almond S, Worrall F, Davies RJ (2016) Assessing the fugitive emission of CH_4 via migration along fault zones – Comparing potential shale gas basins to non-shale basins in the UK. STOTEN. doi.org/10.1016/j.scitotenv.2016.09.052

Ciotoli G, Lombardi S, Zarlenga F (2006) Natural leakage of helium from Italian sedimentary basins of the Adriatic structural margin. perspectives for geological sequestration of carbon dioxide. Advances in the Geological Storage of Carbon Dioxide, 191–202.

Clauser C, Griesshaber E, Neugebauer HJ (2002) Decoupled thermal and mantle helium anomalies: Implications for the transport regime in continental rift zones. J Geophys Res. doi:10.1029/2001JB000675, 2002

Crockett RGM, Perrier F, Richon P (2010) Spectral-decomposition techniques for the identification of periodic and anomalous phenomena in radon time-series. Nat Hazards Earth Syst Sci 10: 559–564

Dehant et al. and Milbert D (2016) Version 15.02.2016 (http://geodesyworld.github.io/SOFTS/solid.htm)

Del Toro I, Berberich GM, Ribbons RR, Berberich MB, Sanders NJ, Ellison AM (2017) Nests of red wood ants (*Formica rufa*-group) are positively associated with tectonic faults: a double-blind test. BioRxiv. doi.org/10.1101/113571

Dèzes P, Schmid SM, Ziegler PA (2004) Evolution of the European Cenozoic Rift System: interaction of the Alpine and Pyrenean orogens with their foreland lithosphere. Tectonophysics 389:1–133

EnergieAgentur NRW (2009) Mine Gas. An energy source in Northrhine-Westphalia. EnergieAgentur NRW 1/2009

Etiope G (2009) Natural emissions of methane from geological seepage in Europe. Atmos Environ 43:1430–1443

Etiope G, Ionescu A (2015) Low-temperature catalytic CO_2 hydrogenation with geological quantities of ruthenium: a possible abiotic CH4 source in chromititerich serpentinized rocks. Geofluids. doi:10.1111/gfl.12106

Etiope G, Judas J, Whiticar MJ (2015) Occurrence of abiotic methane in the eastern United Arab Emirates ophiolite aquifer. Arab J Geosci. doi10.1007/s12517-015-1975-4

Etiope G, Klusman RW (2002) Geologic emissions of methane to the atmosphere. Chemosphere. 49:777-89

Etiope G, Schoell M (2014) Abiotic gas: atypical, but not rare. Elements – An International Magazine of Mineralogy, Geochemistry, and Petrology. doi:10.2113/gselements.10.4.291

Etiope G, Sherwood Lollar B (2013) Abiotic methane on earth. Reviews of Geophysics. doi: 10.1002/rog.20011

Etiope G, Vadillo I, Whiticar MJ, Marques JM, Carreira PM, Tiago I, Benavente J, Jimenez P, Urresti B (2016) Abiotic methane seepage in the Ronda peridotite massif, southern Spain. Applied Geochemistry 66: 101-113

Hinzen KG (2003) Stress field in the Northern Rhine area, Central Europe, from earthquake fault plane solutions. Tectonophysics 377: 325–356

Horita J, Berndt ME (1999) Abiogenic methane formation and isotopic fractionation under hydrothermal conditions, Science. doi:10.1126/science.285.5430.1055

Jackson RB, Down A, Phillips NG, Ackley RC, Cook CW, Plata, DL, Zhao KG (2014) Natural gas pipeline leaks across Washington, DC. Environ. Sci. Technol. 48: 2051–2058

Jílková V, Picek T, Šestauberová M, Krištůfek V, Cajthaml T, Frouz J (2016) Methane and carbon dioxide flux in the profile of wood ant (*Formica aquilonia*) nests and the surrounding forest floor during a laboratory incubation. FEMS Microbiol Ecol. doi.org/10.1093/femsec/fiw141

Keppler F, Boros M, Frankenberg C, Lelieveld J, McLeod A, Pirttilä AM, Röckmann T, Schnitzler JP (2009) Methane formation in aerobic environments. Env Chem. doi.org/10.1071/EN09137

Keppler F, Hamilton JTG, Bra M, Röckmann T (2006) Methane emissions from terrestrial plants under aerobic conditions. Nature. doi:10.1038/nature04420

Kiätävienen R, Purkamo L (2015) The origin, source, and cycling of methane in deep crystalline rock biosphere. Front. Microbiol. doi: 10.3389/fmicb.2015.00725

Kristan M, Leonardis, A, Skočaj, D (2011) Multivariate online kernel density estimation with Gaussian kernels. Pattern Recognition. doi: 10.1016/j.patcog.2011.03.019

LGB RLP (2005) Geologie von Rheinland-Pfalz. Schweizbart'sche Verlagsbuchhandlung. Stuttgart

Litt T, Brauer A, Goslar T, Merk J, Balaga K, Mueller H, Ralska-Jasiewiczowa M, Stebich M, Negendank JFW (2001) Correlation and synchronisation of Lateglacial continental sequences in northern Central Europe based on annually laminated lacustrine sediments. In: Bjorck, S, Lowe, J. J. and Walker M. J. C. (eds) Integration of Ice Core, Marine and Terrestrial Records of Termination 1 from the North Atlantic Region. Quaternary Science Reviews 20:1233–1249

Maes F, Collignon A, Vandermeulen D, Marchal G, Suetens P (1997) Multimodality image registration by maximization of mutual information. IEEE transactions on medical imaging, 16.2: 187-198

Mills C.T, Amano Y, Slater G.F, Dias R.F, Iwatsuki T, Mandernack K.W (2010) Microbial carbon cycling in oligotrophic regional aquifers near the Tono Uranium Mine, Japan as inferred from d13C and D14C values of in situ phospholipid fatty acids and carbon sources. Geochim Cosmochim Acta 74: 3785–3805

Pataki DE, Ehleringer JR, Flanagan LB, Yakir D, Bowling DR, Still CJ, Buchmann N, Kaplan JO, Berry JA (2003) The application and interpretation of Keeling plots in terrestrial carbon cycle research. Global biogeochemical cycles. doi:10.1029/2001GB001850, 2003

Phillips NG, Ackley R, Crosson ER, Down A, Hutyra LR, Brondfield M, Karr JD, Zhao KG, Jackson RB (2013) Mapping urban pipeline leaks: methane leaks across Boston. Environ. Pollut. 173:1–4

Reimann C, Filzmoser P, Garrett RG (2005) Background and threshold: critical comparison of methods of determination. Sci. Total Environ. 346: 1– 16.

491 Ritter JRR (2007) The Seismic Signature of the Eifel Plume. In: Mantle Plumes - A Multidisciplinary
492 Approach. Eds: Ritter, Springer-Verlag Berlin Heidelberg, doi: 10.1007/978-3-540-68046-
493 8_12

494 Ritter JRR, Jordan M, Christensen U, Achauer U (2001) A mantle plume below the Eifel volcanic
495 fields, Germany. Earth Planet. Sci. Lett, 186: 7–14.

496 Saunois M. et al. (2016) The Global Methane Budget: 2000-2012. Earth Syst. Sci. Data Discuss.
497 doi:10.5194/essd-2016-25, 2016

498 Schoell M (1980) The hydrogen and carbon isotopic composition of methane from natural gases of
499 various origins. Geochimica et Cosmochimica Acta. doi:10.1016/0016-7037(80)90155-6

500 Stępniewska Z, Goraj W, Kuźniar A (2014) Transformation of methane in peatland environments.
501 Leśne Prace Badawcze (Forest Research Papers). doi:10.2478/frp-2014-0010

502 Stępniewska Z., Kuźniar A (2013) Endophytic microorganisms – promising applications in
503 bioremediation of greenhouse gases. Appl Microbiol Biotechnol. doi:10.1007/s00253-013-
504 5235-9

505 Tesauro M, Hollenstein C, Egli R, Geiger A, Kahle HG (2006) Analysis of central western Europe
506 deformation using GPS and seismic data. J. Geodynam 42:194-209.

507 Thielemann T, Lucke A, Schleser GH, Littke R (2000) Methane exchange between coalbearing basins
508 and the atmosphere: the Ruhr Basin and the Lower Rhine Embayment, Germany. Org
509 Geochem 31:1387-1408

510 Toutain JP., Baubron JC (1999) Gas geochemistry and seismotectonics: A review. Tectonophysics
511 304:1-27

512 Trinkwasserverordnung in der Fassung der Bekanntmachung vom 10. März 2016 (BGBl. I S. 459), die
513 durch Artikel 4 Absatz 21 des Gesetzes vom 18. Juli 2016 (BGBl. I S. 1666) geändert
514 worden ist

515 Walker KT, Bokelmann GHR, Klemperer SL, Bock G (2005) Shear-wave splitting around the Eifel
516 hotspot: Evidence for a mantle upwelling. Geophys J Int 163: 962–980

517 Whiticar MJ (1999) Carbon and hydrogen isotope systematics of bacterial formation and oxidation of
518 methane. Chem Geol 161: 291-314

519 Zazzeri G, Lowry D, Fisher RE, France JL, Butler D, Lanoisellé M, Nisbet EG (2017) Identification of
520 urban gas leaks and evaluation of methane emission inventories using mobile
521 measurements. Geophysical Research Abstracts. Vol. 19, EGU2017-14409, 2017

522 Ziegler P A., Dèzes P (2005) Crustal Evolution of Western and Central Europe. Crust Europe
523 20.03.05, 31 p.